CrossMark

Wilson cycle passive margins: Control of orogenic inheritance on continental breakup

Kenni D. Petersen [a,*], Christian Schiffer [a,b]

[a] Department of Geoscience, Aarhus University, 8000 Aarhus, Denmark
[b] Department of Earth Sciences, Durham University, Durham DH1 3LE, United Kingdom

A B S T R A C T

Rifts and passive margins often develop along old suture zones where colliding continents merged during earlier phases of the Wilson cycle. For example, the North Atlantic formed after continental break-up along sutures formed during the Caledonian and Variscan orogenies. Even though such tectonic inheritance is generally appreciated, causative physical mechanisms that affect the localization and evolution of rifts and passive margins are not well understood.

We use thermo-mechanical modeling to assess the role of orogenic structures during rifting and continental breakup. Such inherited structures include: 1) Thickened crust, 2) eclogitized oceanic crust emplaced in the mantle lithosphere, and 3) mantle wedge of hydrated peridotite (serpentinite).

Our models indicate that the presence of inherited structures not only defines the location of rifting upon extension, but also imposes a control on their structural and magmatic evolution. For example, rifts developing in thin initial crust can preserve large amounts of orogenic serpentinite. This facilitates rapid continental breakup, exhumation of hydrated mantle prior to the onset of magmatism. On the contrary, rifts in thicker crust develop more focused thinning in the mantle lithosphere rather than in the crust, and continental breakup is therefore preceded by magmatism. This implies that whether passive margins become magma-poor or magma-rich, respectively, is a function of pre-rift orogenic properties.

The models show that structures of orogenic eclogite and hydrated mantle are partially preserved during rifting and are emplaced either at the base of the thinned crust or within the lithospheric mantle as dipping structures. The former provides an alternative interpretation of numerous observations of 'lower crustal bodies' which are often regarded as igneous bodies. The latter is consistent with dipping sub-Moho reflectors often observed in passive margins.

© 2016 Published by Elsevier B.V. on behalf of International Association for Gondwana Research.

1. Introduction

Passive margins form the transition between oceanic and continental lithosphere and are the result of rifting and continental break-up. These processes represent one phase of the Wilson cycle (Wilson, 1966; Dewey and Spall, 1975) where continents recurrently disintegrate and reassemble and oceanic crust and lithosphere form, subduct and recycle, a process that is likely to have been ongoing for around 3 Ga (Cawood, 2006; Shirey and Richardson, 2011). The present-day margins of the Central and North Atlantic are a manifestation of at least two complete Wilson cycles: The supercontinent of Rodinia was assembled at the end of the Mesoproterozoic Grenvillian orogeny (Piper, 2000; Thomas, 2006), which after break-up was divided by the newly forming Iapetus Ocean. The closure of the Iapetus Ocean leads to the Paleozoic Caledonian–Acadian orogeny in the North Atlantic

region. This continent–continent collision involved the continents Laurentia, Baltica, Avalonia and further smaller continental fragments and terranes (Van Staal et al., 1998; Leslie et al., 2008) and formed a coherent, Himalaya-type mountain range of at least 3000 km length and 1000 km width (Roberts, 2003; Gee et al., 2008). The subsequent Late Paleozoic Variscan orogeny assembled large parts of present day Central and Southern Europe partly overprinting the Caledonian Orogen in the Appalachians (Stamfli and Kozur, 2006). Most recently, Mesozoic and Cenozoic rifting caused the breakup of the supercontinent Pangea and the formation of the North Atlantic and passive margins (Skogseid et al., 2000).

Remnant structures and lineaments of earlier mountain-building events are generally strike-parallel and mimic the present-day North Atlantic margins, implying ancestral control of the older orogens (Williams, 1995 and references therein). In a recent review by Buiter and Torsvik (2014) it is concluded that continental breakup generally occurs along former collision zones irrespective of their age. In another recent paper, Schiffer et al. (2015b) demonstrated that the plate tectonic

* Corresponding author.
  E-mail address: kenni@geo.au.dk (K.D. Petersen).

evolution of the North Atlantic region is likely controlled by inherited orogenic structures formed during the Caledonian.

Despite general agreement that orogenic structures can control the location of extension (e.g. Dunbar and Sawyer, 1989; Williams, 1995), few studies quantitatively address possible implications of orogenic inheritance during the formation and evolution of passive margins. In this paper we explore such implications using numerical modeling of the rift-to-drift evolution that forms as a result of extension of lithosphere with rheological inhomogeneities inherited from the time of suturing and orogeny. We investigate what influence such structures have on structural properties and the evolution of passive margins. These include the asymmetry of conjugate margins, the formation of lower crustal bodies (LCBs) of different shapes, hyperextension, formation of blocks of thinned continental crust (Péron-Pinvidic and Manatschal, 2010; Lundin and Doré, 2011) and the rate and timing of melt generation. Before describing our modeling procedure and our results, we first present a general summary of such properties of passive margins.

2. Magma-rich vs. magma-poor margins

Passive margins accommodate the transitional thinning of the continental crust towards the oceanic sea floor (Fig. 1) and are often discriminated in terms of the volume of igneous rocks emplaced during thinning of the continental crust. The Iberia–Newfoundland conjugate margins (Fig. 1e–g) represent a much cited example of a conjugate pair of magma-poor margins. Here, igneous rocks are absent or sparse (Minshull et al., 1998), and blocks of thinned continental crust are in tectonic contact with exhumed and serpentinized mantle ('extensional allochthons'; see Wernicke, 1981; Froitzheim and Manatschal, 1996; Péron-Pinvidic and Manatschal, 2010). The exhumed mantle forms a distal zone that gradually transitions to 'normal' oceanic crust (Boillot et al., 1980; Bown and White, 1994; Reston and Morgan, 2004;

Péron-Pinvidic and Manatschal, 2010). In contrast, magma-rich passive margins, such as the Greenland–Scotland/Norway margins (Fig. 1a–c), are associated with abundant igneous rocks in the form of subaerial and submarine extrusive basalt flows (Mutter et al., 1982; Tegner et al., 1998) or lower crustal intrusions (White, 1992; Coffin and Eldholm, 1994; Menzies, 2002). The total thickness of igneous rocks is, at places, reported to be several times the thickness of normal oceanic crust (Kelemen and Holbrook, 1995; Korenaga et al., 2000).

An apparent difference between magma-rich and magma-poor margins is that the onset of melt production tends to precede complete breakup of the continental lithosphere during the formation of magma-rich margins, forming igneous intrusions in and flood basalts on top of continental crust. The opposite seems to be the case for magma-poor margins (Manatschal et al., 2015), where no or few igneous products are emplaced in or on the thinned continental crust. Igneous rocks instead appear to have formed after the crust was completely thinned and mature oceanic spreading onset.

A number of models have been invoked to account for the differences between the two types of margins. For example, Reston and Morgan (2004) suggested that magma-poor margins can be explained by a ~100 °C reduction of mantle temperature relative to the 'normal' ~1300 °C, typically required to produce 6–7 km oceanic crust (e.g. Bown and White, 1994). Similarly, to explain magma-rich margins, hotter-than-normal mantle temperatures have been invoked, such as plumes (White and McKenzie, 1989). The plume-origin of Large Igneous Provinces and associated magma-rich margins has been disputed (Holbrook et al., 2001; Foulger et al., 2005; Foulger and Jurdy, 2007). Alternative mechanisms include small-scale convection (Mutter et al., 1988; King and Anderson, 1998; Boutilier and Keen, 1999), time/depth-dependent thinning of the lithosphere (van Wijk et al., 2001), enhanced melt source fertility (Korenaga and Kelemen, 2000; Korenaga, 2004) and water in the mantle source (Jamtveit et al., 2001).
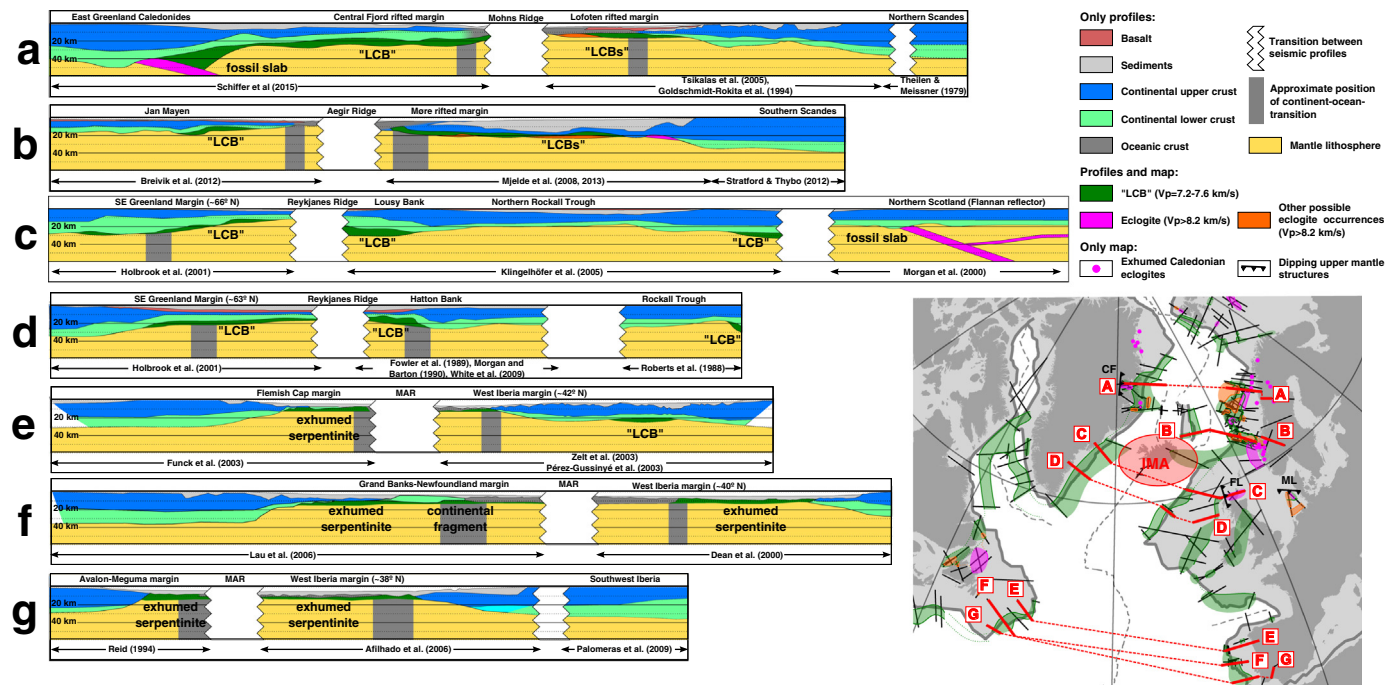

Fig. 1. North Atlantic Crustal Transects from the East Greenland–Norwegian (a–b), East Greenland–British (c–d) and Iberia–Newfoundland margins (e–g). The transects show sediments (gray), basalts (red), upper and lower crust (dark and light blue) as well as lower crustal bodies of different kind. Magenta shows previously interpreted eclogite bodies; orange shows other areas with Vp > 8.2 km/s at the base of the crust, which may be attributed to the presence of eclogite; green shows lower crustal bodies consistent with mafic underplating or serpentinite bodies. The map illustrates the position of the transects (red) and wide-angle seismic lines (black lines) in the North Atlantic. Magenta, orange and green are the same as for the transects. IMA — Iceland Melt Anomaly. CF — Central Fjord structure. ML — Mona Lisa structure. FL — Flannan structure. (For interpretation of the references to color in this figure legend, the reader is referred to the web version of this article.)

Many magma-rich margins are characterized by lower crustal bodies (LCBs) with higher than normal crustal and sometimes also mantle velocities and densities. A number of different models for the formation and composition of such structures have been proposed, although most commonly these are associated with rift-magmatism (e.g. Olafsson et al., 1992; Ren et al., 1998; White et al., 2008; Thybo and Artemieva, 2013).

During the recent decade a number of alternative models of the nature of LCBs have been proposed. For example, LCBs with higher than normal mantle velocities (e.g. Fig. 1a–c) have been interpreted as eclogite bodies genetically linked to earlier suturing events (e.g. Fig. 1a; Gernigon et al., 2006; Mjelde et al., 2013b). Similarly, dipping sub-crustal velocity anomalies along the margins of East Greenland and Scotland, respectively, (Fig. 1a,c) have been interpreted as relict, eclogitized subduction zones formed during the Caledonian orogeny or earlier orogenies (Snyder and Flack, 1990; Warner et al., 1996; Schiffer et al., 2015a). An Appalachian origin has been suggested for dipping mantle structures found in Newfoundland (Hall et al., 1990; van der Velden et al., 2004).

LCBs with lower than normal mantle seismic velocities (but higher than for normal lower crust) at the magma-rich Norwegian passive margins (e.g. Fig. 1a,b) have also been interpreted as hydrated (serpentinized) mantle (Ren et al., 1998; Mjelde et al., 2002). Similarly as for magma-poor margins (see below), this is commonly explained by syn-rift mantle hydration and serpentinization (Péron-Pinvidic and Manatschal, 2009). An alternative mechanism for the presence of serpentinite in the Northern North Sea was hypothesized by Fichler et al. (2011) who suggested the possibility that water was supplied by fluids present in the crust before breakup by slab dehydration during the Caledonian orogeny.

The LCBs at magma-rich margins often share similar geophysical properties with those of exhumed and serpentinized mantle at magma-poor margins and are potentially difficult to distinguish with geophysical methods (Mjelde et al., 2002).

At magma-poor margins high velocity bodies have been associated with serpentinite exposed directly at or near the seafloor (Boillot et al., 1980; Brun and Beslier, 1996; Eddy et al., 2013). A commonly accepted model for the formation of such bodies assumes that they represent exhumed mantle that was hydrated in-situ by hydrothermal circulation facilitated by permeability generated by rift-related faulting (Pérez-Gussinyé and Reston, 2001). An often observed gradual increase into velocities greater than 8.1 km/s has been attributed to downward decreasing serpentinization (Péron-Pinvidic and Manatschal, 2009).

The width of both magma-rich and magma-poor margins varies from <100 km to more than 500 km (Péron-Pinvidic and Manatschal, 2010; Lundin and Doré, 2011), and margin conjugates often display strong asymmetry (Lister et al., 1986). During the last 30 years it has been demonstrated that numerous physical mechanisms can account for the variability of margin width and asymmetry, respectively (e.g. England, 1983; Buck, 1991; Brune et al., 2014).

Some margins, often referred to as 'hyperextended' (Manatschal, 2004), display extensional allochthons, isolated crustal blocks of continental material separated by windows of exhumed mantle (Péron-Pinvidic and Manatschal, 2010). Other authors use this expression to describe highly stretched, but not entirely failed continental crust of passive margins (Lundin and Doré, 2011; Brune et al., 2014).

3. Methods

3.1. Overview

We employ a 2D thermo-mechanical model of elastic, viscous and plastic deformation to simulate extension of an orogen.

Because we here investigate how rifting localizes along former suture zones as part of the Wilson cycle, we depart from the traditional approach to 'seed' the rift localization by a minor perturbation of an otherwise 1D initial structure (e.g. Huismans and Beaumont, 2011; Brune et al., 2014). Instead, we attempt to simulate the onset of rifting in a setting that represents the lithosphere-scale structure of an old suture, as it may have been rendered several 100 Ma after the latest suturing event. For this we introduce three rheologically important components in the initial setup of our model, which represent important properties of subduction zones (Duesterhoeft et al., 2014) and orogens:

1) Thickened crust, 2) a dipping fossil eclogite layer and 3) a remnant hydrated mantle wedge.

Our reasons for including these components are the following:

1) Increased crustal thickness is a well-known property of orogens (e.g. Christensen and Mooney, 1995). Pre-rift crustal thickness has been shown to affect the 'mode' of rifting (Buck, 1991), and is therefore considered a variable in this study. The observed ambient pre-rift continental crustal thicknesses seem to be larger in Greenland and Scandinavia (up ~50 km) than observed in Britain, Newfoundland and Iberia where proximal crustal thickness is in the order of 35 km (Fig. 1).

2) Dipping mantle structures of possible eclogite have not only been preserved along present-day passive margins, as mentioned above (e.g. Fig. 1a,c), but also appear to correlate well with sutures that have not been subsequently extended to form passive margins (Balling, 2000; van der Velden and Cook, 2005). Eclogite is rheologically different from peridotite (Fig. 2; Karato and Wu, 1993; Zhang and Green, 2007) and has higher density (Aoki and Takahashi, 2004).

3) As a result of subduction prior to continent–continent collision vast amounts of water are released from the subducting oceanic lithosphere into the above mantle wedge. Thermodynamic models coupled with pore-fluid transport and seismological studies indicate that this leads to pervasive hydration of the mantle wedge (Iwamori, 1998; Bostock et al., 2002; Kawakatsu and Watada, 2007). Such studies indicate that the subducting plate releases water to the above mantle wedge from depths of at least 100 km.

The initial setup of the models presented here (Fig. 2) is based on the assumption that orogenic components are present long after the cessation of compressional tectonics (Schiffer et al., 2015b). It is assumed that remnant subducted slab material below the continental lithosphere has detached (e.g. Duretz et al., 2011), and that the thermal state of the lithosphere (thickness: 150 km) is in conductive equilibrium with an isentropic mantle with a potential temperature of 1325 °C. Within a mantle lithosphere with olivine rheology (Table 1) the presence of an eclogitized remnant of a fossil slab with an assumed thickness of 15 km and dip of 20, 25 or 30° is assumed. These values are within the range of recent subduction zone geometries (e.g. Cruciani et al., 2005). Furthermore, a remnant mantle wedge with serpentinite rheology (Hilairet et al., 2007) is present above the fossil slab down to depth of 100 km and below the continental crust. The initial thickness of continental crust is 35, 40, 45, 50 or 55 km. Serpentinite is only stable at certain P–T conditions (Ulmer and Trommsdorff, 1995), corresponding to depths of 50–60 km at initial conditions (Fig. 2b–d). Crustal thickness and the subduction angle thereby control the size of the serpentinite stability window, geometrically and thermally due to crustal heat production and burial.

3.2. Thermo-mechanical model

Our numerical method is generally similar to that presented by Gerya and Yuen (2007), but differs by employing a multigrid-based approach (Petersen et al., 2010; Petersen et al., 2015) which allows for high resolution simulation in both space and time. The applied method for solving the coupled equations for conservation of mass (assuming incompressibility), energy and momentum (Gerya and Yuen, 2007) is described in greater details in Petersen et al. (2015 and references

therein) and accounts both for viscous deformation (dislocation and diffusion creep), shear elasticity and plastic ('brittle') deformation:

$$\dot{\varepsilon}'_{ij} = \dot{\varepsilon}'_{ij(diffusion)} + \dot{\varepsilon}'_{ij(dislocation)} + \dot{\varepsilon}'_{ij(elastic)} + \dot{\varepsilon}'_{ij(plastic)}$$

$$= \frac{1}{2\eta_{(diffusion)}} \sigma'_{ij} + \frac{1}{2\eta_{(dislocation)}} \sigma'_{ij} + \frac{1}{2\mu} \frac{D\sigma'_{ij}}{Dt} + \chi \frac{\sigma'_{ij}}{2\sigma_{II}}$$

$\dot{\varepsilon}'_{ij}$ is the total strain rate tensor, σ_{ij}' is the deviatoric stress tensor, σ_{II} is the square root of the second invariant of the latter, η is viscosity, μ is elastic shear modulus, χ is a plastic multiplier that is nonzero only if $\sigma_{II} = \sigma_{yield}$, where $\sigma_{yield} = C + P\sin(\phi)$ is the cohesion (C), friction angle (φ) and pressure (P)-dependent Mohr–Coulomb failure limit. Viscosity parameters depend on lithology, temperature T, pressure, P, and stress σ_{II} (second invariant of the deviatoric stress tensor) as: $\eta = \frac{1}{2A\sigma_{II}^{n-1}} \exp(\frac{E+PV}{\underline{R}} T)$. E is activation energy, V is activation volume, and $\underline{R}$ is the gas constant.

The relevant parameters for each lithology are given in Table 1.

The extension models presented here have a grid resolution of 850 m for the entire 2000 km × 600 km modeling domain and are either run for up to 50 Ma (at 2 cm/a extension) or 200 Ma (at 0.5 cm/a extension). To simulate localized brittle deformation, the friction angle is reduced linearly to 0 with plastic strain until the latter reaches 0.5. A stress-free surface is represented by employing a 'sticky-air' approach (Crameri et al., 2012) by letting the initial upper 40 km of the modeling domain to have little mass and low (relative to the Ma-scale of the rift-to-drift process) viscosity of 10^{20} Pa s. Furthermore, we ensure that negligible stresses form at the surface by also setting a plastic yield limit of 0.1 MPa (similar to the numerical precision of the modeling method) for the 'air' layer (Petersen et al., 2015). This renders the surface effectively stress-free even during rapid surface movements and dynamically reduces the effective viscosity only when needed (a beneficial property for especially iterative thermo-mechanical solution strategies).

3.3. Melt model

Incremental production of melt due to decompression of mantle rocks is calculated in a separate sub step during each time step after velocity, pressure and temperature fields and advection of the latter have

been determined. The first step is similar to earlier approaches (Gerya and Yuen, 2007; Petersen et al., 2010) and solves the coupled equations for conservation of mass and momentum. The temperature calculation during the first step assumes that melting does not occur. If the temperature then exceeds a depletion- and pressure-dependent solidus (assuming batch melting (Scott, 1992)), a melt increment and corresponding temperature change is calculated. The solidus T_s is calculated following Katz et al. (2003), assuming a source composition with 17% clinopyroxene and no water. If non-melting effects (adiabatic, shear, radiogenic and conductive heating) would lead to a temperature increase $\Delta T = T' - T_s > 0$ above the solidus, an increment of melt fraction, ΔF, is calculated in a second step by assuming that melting is a temporarily isentropic (Scott, 1992; Phipps Morgan and Morgan, 1999) and isobaric (Nielsen and Hopper, 2004) process: $\Delta F = \frac{\Delta T}{\frac{L}{C_p} + \frac{\partial T_s}{\partial F}}$. Here, $L = T\,\Delta S$ is latent heat capacity where ΔS is entropy change due to melting, and C_p is isobaric specific heat capacity.

The temperature change due to melting is the corresponding change in solidus temperature (Phipps Morgan and Morgan, 1999):

$$dT = dT_s = \frac{\partial T_s}{\partial F} \Delta F$$

Changes in depletion and associated temperature changes are updated for each material point which is advected in accordance with the solid velocity field during each time step. Inspired by Ito et al. (1996) we simulate melt extraction by calculating the total mass of melt produced within the entire modeling domain during a time step: $M_{melt} = \iint \Delta F dx dz$. This mass is assumed to be immediately extracted and brought to the surface as a lava flow with a Gaussian thickness distribution, d, and total cross sectional area that corresponds to the area of the produced melt: $d = \frac{\rho_m}{\rho_b} M_{melt} \frac{1}{2c\sqrt{2\pi}} \exp\left(-\frac{(x-x_0)^2}{2c^2}\right)$ where $\frac{\rho_m}{\rho_b}$ is the ratio between mantle source and solidified melt density which, for simplicity, is assumed to be 3300/3000. The constant c defines a length scale for a lava flow and is assumed to be 25 km. The lateral source position x_0 is assumed to equal the lateral position of the shallowest melt producing point in the mantle during the given time step. The deposition of lava flows is implemented in the thermo-mechanical model by converting material points that were initially 'air' to a lithology with a plagioclase-like (Ranalli, 1995) flow law (see Table 1).
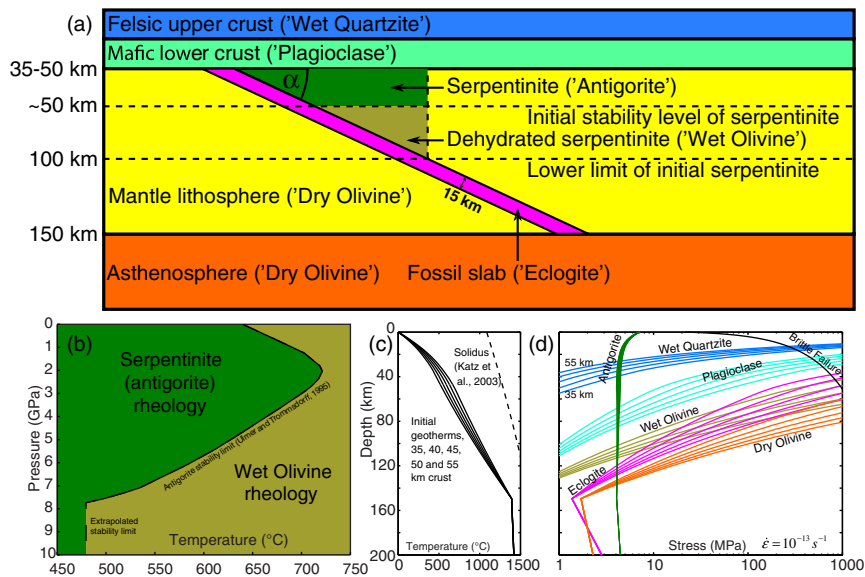

Fig. 2. a, Initial model setup. b, Stability limit for serpentinite. c, Initial lithosphere geotherms for different crustal thicknesses. Dashed line indicates assumed pressure-dependent solidus for fertile asthenospheric mantle (Katz et al., 2003). d, Constant strain rate (10^{-13} s^{-1}) stress profiles for ductile creep in the different lithologies employed in this study. Different curves for each lithology show the effect of different initial crustal thickness (corresponding to geotherms shown in c). Black line indicates brittle yield stress. Rheological parameters are shown in Table 1.

Table 1
Assumed model parameters.

Description	Symbol	Value
Freely deforming upper layer		
Viscosity	η	10^{20} Pas
Yield strength	σ_y	0.1 MPa
Shear modulus	μ	25 GPa
Density	ρ	1 kg m^{-3}
All rocks		
Angle of internal friction (Buiter et al., 2006)	φ	36° (linearly reduced to 0° as plastic strain approaches 0.5)
Cohesion (Ranalli, 1995)	C	22 MPa
Crust		
Coefficient of thermal expansion (Parsons and Sclater, 1977)	A	$3.28 \cdot 10^{-5}$ K^{-1}
Thermal conductivity	K	2.5 W m^{-1} K^{-1}
Isobaric heat capacity	C_p	800 J kg^{-1} K^{-1}
Shear modulus	μ	25 GPa
-Upper ('wet quartzite')		
Reference density at 273 K	ρ_0	2750 kg m^{-3}
Radiogenic heat production	H_r	1.0 µW m^{-3}
Activation energy (Ranalli, 1995)	E	154 kJ mol^{-1}
Power-law exponent (Ranalli, 1995)	N	2.3
Power-law constant (Ranalli, 1995)	A	$5.07 \cdot 10^{-18}$ Pa^{-n} s^{-1}
-Lower ('plagioclase')		
Reference density at 273 K	ρ_0	2900 kg m^{-3}
Radiogenic heat production	H_r	0.75 µW m^{-3}
Activation energy (Ranalli, 1995)	E	238 kJ mol^{-1}
Power-law exponent (Ranalli, 1995)	n	3.2
Power-law constant (Ranalli, 1995)	A	$2.08 \cdot 10^{-23}$ Pa^{-n} s^{-1}
-Specific for volcanic sediments (otherwise like lower crust)		
Reference density at 273 K	ρ_0	3000 kg m^{-3}
Thermal conductivity	k	2.0 W m^{-1} K^{-1}
Mantle		
Coefficient of thermal expansion (Gillet et al., 1991)	α	$2.77 \cdot 10^{-5}$ K$^{-1} + 0.97 \cdot 10^{-8}$ K^{-2} T + 0.32 K T^{-2}
Thermal conductivity (McKenzie et al., 2005)	k	4.08 W m^{-1} K^{-1}(298 K/T)$^{0.406}$
Isobaric heat capacity (Berman and Brown, 1986)	C_p	$[1.69 \cdot 10^{-3} - 1.42 \cdot 10^4(T/K)^{0.5} - 8.27 \cdot 10^8(T/K)^{-3}]$ J kg^{-1} K^{-1}
Shear modulus (Karato and Wu, 1993)	μ	80 GPa
-Standard mantle ('dry olivine')		
Reference density at 273 K	ρ_0	3333 kg m^{-3}
Activation energy (dislocation creep) (Karato and Wu, 1993)	E	540 kJ mol^{-1}
Power-law exponent (dislocation creep) (Karato and Wu, 1993)	n	3.5
Power-law constant (dislocation creep) (Karato and Wu, 1993)	A	$2.41 \cdot 10^{-16}$ Pa^{-n} s^{-1}
Activation volume (dislocation creep) (Karato and Wu, 1993)	V	15 cm^3 mol^{-1}
Power-law exponent (diffusion creep) (Karato and Wu, 1993)	n	1
Power-law constant (diffusion creep) (Karato and Wu, 1993)	A	$1.92 \cdot 10^{-11}$ Pa^{-1} s^{-1}
Activation volume (diffusion creep) (Karato and Wu, 1993)	V	6 cm^3 mol^{-1}
-Dehydrated serpentinite 'Wet Olivine'		
Reference density at 273 K	ρ_0	3333 kg m^{-3}
Activation energy (dislocation creep) (Karato and Wu, 1993)	E	430 kJ mol^{-1}
Power-law exponent (dislocation creep) (Karato and Wu, 1993)	n	3.0
Power-law constant (dislocation creep) (Karato and Wu, 1993)	A	$3.90 \cdot 10^{-15}$ Pa^{-n} s^{-1}
Activation volume (dislocation creep) (Karato and Wu, 1993)	V	15 cm^3 mol^{-1}
Power-law exponent (diffusion creep) (Karato and Wu, 1993)	n	1
Power-law constant (diffusion creep) (Karato and Wu, 1993)	A	$2.92 \cdot 10^{-11}$ Pa^{-1} s^{-1}
Activation volume (diffusion creep) (Karato and Wu, 1993)	V	6 cm^3 mol^{-1}
-Serpentinite ('antigorite')		
Reference density at 273 K	ρ_0	3233 kg m^{-3}
Activation energy (Hilairet et al., 2007)	E	89 kJ mol^{-1}
Power-law exponent (Hilairet et al., 2007)	n	3.8
Power-law constant (Hilairet et al., 2007)	A	$3.12 \cdot 10^{-37}$ Pa^{-n} s^{-1}
Activation volume (Hilairet et al., 2007)	V	3.2 cm^3 mol^{-1}
-Fossil slab ('eclogite')		
Reference density at 273 K	ρ_0	3400 kg m^{-3}
Activation energy (Zhang and Green, 2007)	E	403 kJ mol^{-1}
Power-law exponent (Zhang and Green, 2007)	n	3.5
Power-law constant (Zhang and Green, 2007)	A	$2.00 \cdot 10^{-18}$ Pa^{-n} s^{-1}
Activation volume (Zhang and Green, 2007)	V	27.2 cm^3 mol^{-1}

Reference density, ρ_0 of mantle rocks is assumed to decrease with increasing melt depletion F, following Petersen et al. (2015) and Phipps Morgan (1997), by a factor d, given by: d = (1 + 29erf(20F))exp(8.02F).

3.4. Serpentinite model

Serpentine minerals are only stable at a limited range of temperatures and pressures. The high-temperature phase, antigorite, dehydrates and forms olivine and orthopyroxene at temperatures above 500–700 °C, depending on pressure (Ulmer and Trommsdorff, 1995). To represent this effect, we employ a simple binary and one-way phase model for serpentinite (Fig. 2b). Our phase model is digitized from Ulmer and Trommsdorff (1995) and only involves transformation of serpentinite to olivine mantle, assuming that water escapes instantaneously during dehydration, preventing the reverse reaction. However, since trace amounts of water can be present within olivine, significantly reducing its strength (e.g. Mei and Kohlstedt, 2000), we assume a 'Wet Olivine' rheology for dehydrated serpentinite. According to the phase diagram of Ulmer and Trommsdorff (1995) the breakdown of serpentinite at pressures <~2 GPa involves a transitional reaction where talc and orthopyroxene are formed and remain stable within a temperature interval of up to ~150 °C. For simplicity this phase assemblage is assumed to have mechanical properties (viscosity and density) that are similar to serpentinite. Serpentinite is assumed to have temperature, pressure and stress-dependent viscosity as constrained by laboratory experiments on antigorite (Hilairet et al., 2007).

3.5. Modeling procedure

In total we conduct 40 experiments in order to explore the effect of parameters that may control the rift-to-drift evolution of passive margins along former sutures. These experiments include all possible combinations of models with initial crustal thickness of 35, 40, 45, 50 or 55 km, dip of fossil slab of 20, 25 or 30°, and with imposed boundary extension rates (full-rate) of either 2 cm/a or 0.5 cm/a. For reference, a set of models without an initial fossil slab and mantle wedge is also calculated. These models are instead 'seeded' with a Gaussian perturbation of the thermal lithosphere thickness with amplitude of 10 km and 'standard deviation' of 100 km in the center of the modeling domain. All models are run until continental breakup (here defined as the time where crustal thinning factor, β, somewhere reaches 100) plus the time required for additional 200 km extension (i.e. 10 or 40 Ma, depending on extension rate). However, in some settings breakup may occur very late, and therefore simulations are stopped if extension reaches 1000 km (i.e. at 50 or 200 Ma for the two extension rates).

4. Results

4.1. Thin crust — serpentinite flow

The evolution of an extension model with relatively thin initial crust (35 km), an initial slab dip of 30°, and imposed extension rate of 2 cm/a is presented in Fig. 3. In this model the initial P–T conditions for serpentinite stability (Fig. 2b) reach a depth of ~65 km. This allows for a relatively large amount of pre-rift serpentine, as compared to thicker crust (Figs. 4–6), because thin crust 1) leaves more space for serpentinite, and 2) causes less radiogenic heat production and therefore a colder lithospheric mantle. Consequently, the large amount of weak and buoyant serpentinite controls the rift localization in the crust, and within 3.5 Ma, the crust is completely thinned (crustal thinning factor, $\beta > 100$), and serpentinite is buoyantly exhumed to the surface. At this stage, the lithospheric mantle has only been thinned by a factor of less than 2, and decompression melting has not yet onset. After continental breakup, serpentinite exhumation continues while the lithospheric mantle is thinning. At ~4.5 Ma, decompression melting within the mantle onsets and steadily increases until 10 Ma where a near-steady state magmatic crust production (expressed as the volumetric melt production rate divided by the extension rate, v: $h_c = \frac{\rho_m M_{melt}}{\rho_b v}$) reaches a thickness of ~7 km (Fig. 5). The eclogite in the fossil

slab is rheologically similar to the olivine-rich rocks of the lithosphere compared to the much weaker serpentinite (Fig. 2c), and is generally deformed coherently along with the surrounding mantle lithosphere. Therefore, after breakup, when deformation within the conjugate margins has effectively ceased, the slab has been rifted apart along with the lithospheric mantle. On the left margin, the slab is rendered almost undeformed to a depth of ~55 km and therefore essentially retains its original dip of 30° (however, isostatic effects of crustal thinning have regionally rotated the slab reducing its dip by ~3°). The initially deeper part of the slab left within this margin has been deformed due to lithospheric thinning and brought to depths at or near the base of the tapering crust. On the conjugate (right) margin, the remaining slab (which was initially at depths below 100 km) has been thinned along with mantle lithosphere, and forms a sub-linear structure with a dip of ~45°. At the onset of the simulation, the deepest part of the fossil slab drips off the lithosphere and sinks into the asthenosphere. This is a consequence of the assumed higher density of eclogite ($+66$ kg/m^3). However, at slightly shallower depths (ca. 130 km), the lower temperatures stabilize the slab (and its surroundings), and deformation above this depth is primarily due to rifting. Thinning of the continental crust is generally decoupled from the lithosphere below due to the weak serpentinite layer. As a result, the transition from unthinned to completely thinned crust is relatively abrupt, but also laterally displaced from where the mantle lithosphere is thinned the most during crustal breakup (Fig. 3). On either margin much of the original serpentinite is preserved as 10–20 km thick bodies directly below the transitional oceanic crust or the thinned continental crust.

4.2. Thick crust — crustal flow

Models with greater initial crustal thickness show a different evolution where magmatism onsets long before continental breakup. For initial crust greater than 45 km (and extension rate of 2 cm/a) melting onsets at a stage when the crust has been thinned by 1.5–1.7 (Fig. 5). In these settings, less serpentinite is initially present due to the deeper crust and hotter uppermost mantle, and the crust flows more readily. This causes strain to localize more rapidly within the mantle lithosphere and leads to faster thinning as compared to the crust. The crust, on the contrary, flows internally towards the lower potential within the rift axis, counteracting crustal thinning (e.g. Buck, 1991). An example of this is presented in Fig. 6 where initial crustal thickness and slab angle are 45 km and 30°, respectively. In this setting, only a thin layer of serpentinite is initially present, strain localizes rapidly, and the mantle lithosphere is thinned sufficiently for melting to onset after 6 Ma. During the same period of time, the crust is thinned less and over a wider region. Within the next 5 Ma (6–11 Ma from the beginning of the simulation), the mantle lithosphere is almost completely thinned and the melt production reaches ~6 km, close to the steady state productivity, whereas the crust is thinned by up to a factor of ~10 (Fig. 5). After this stage, the mode of 6 km melt production continues along with delocalized crustal thinning where the thinning factor does not locally exceed 10 until continental breakup at ca. 25 Ma. The resulting set of conjugate margins are strongly asymmetric with continental crust on one side tapering from 0 to the original 45 km over a lateral distance of ~600 km, whereas the crust of the conjugate margin thins within a distance of less than ~100 km. Both margins show continental crust covered by rift-related volcanics. This is caused by early magmatism before crustal breakup and is seen in all models with initial crust greater than 40 km (Figs. 5–6).

4.3. Effect of extension rate

Figs. 7–8 show passive margin models and melt productivity, respectively for an extension rate of 0.5 cm/a. Models with this boundary condition are generally similar to the models with faster extension, but differ in the sense that the abovementioned effects of initial crustal
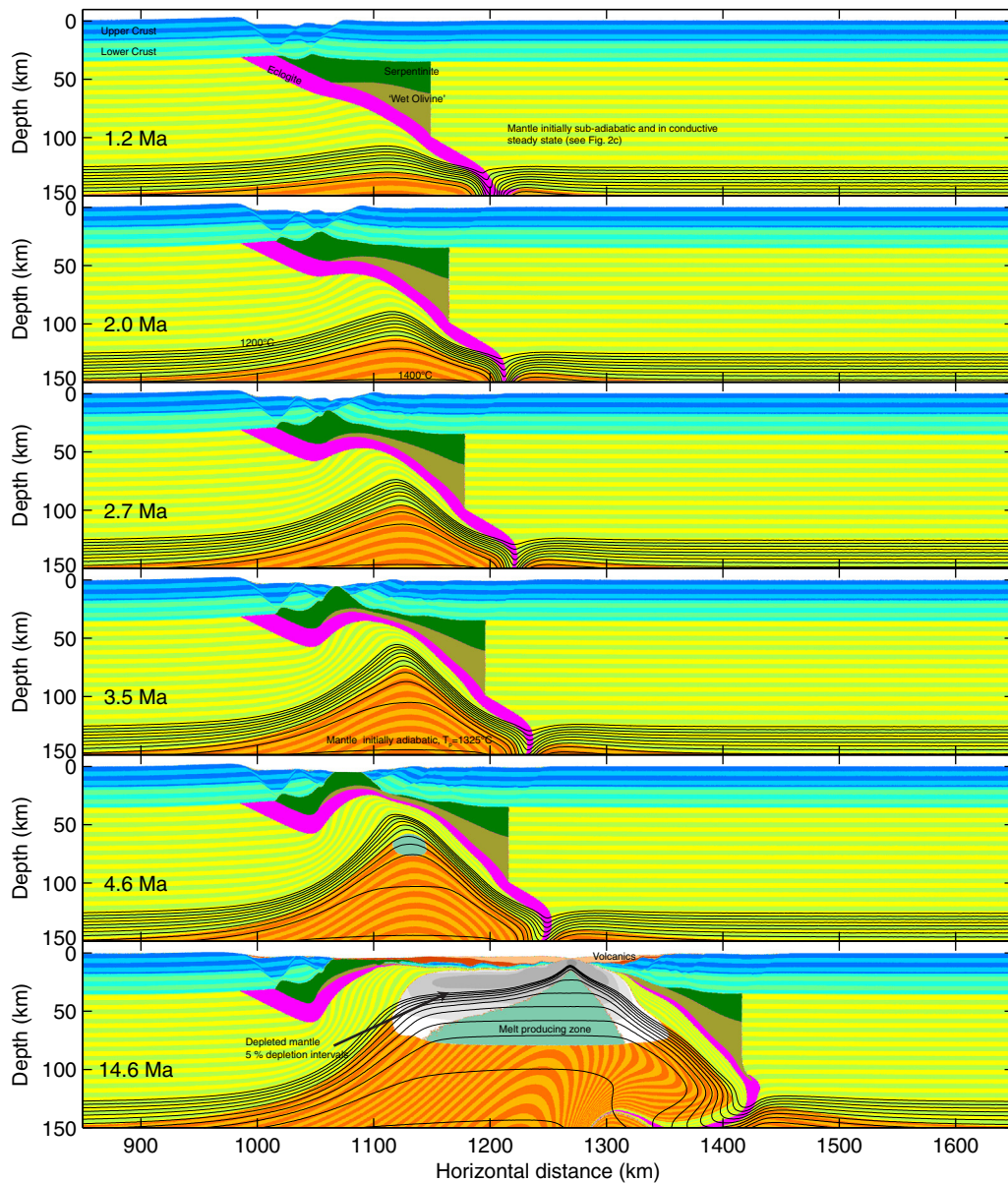
Fig. 3. Evolution of model with initially 35 km crust and fossil slab dip of 30°. Extension rate is 2 cm/a. Colors are similar to those in Fig. 2, but horizontal color striping of the initial state is used to highlight deformation. Black lines are isotherms for temperatures of 1200 °C and above with intervals of 20 °C. Light blue indicates the active melt-producing zone in the mantle, and gray tones indicate where mantle melting has occurred at some stage. Different gray tones represent 5% intervals of melt depletion which increases with decreasing brightness. Topmost layers with salmon/orange-like colors are volcanics deposited at the surface. Color changes within the volcanics represent isochrons spaced with 5 Ma. (For interpretation of the references to color in this figure legend, the reader is referred to the web version of this article.)

thickness on the rate and distribution of thinning are more pronounced. For example, in the models with 35 km initial crust, serpentinite is also exhumed to the seafloor, but over a greater width (~100 km) as compared to the faster spreading case. Similarly, the models with thicker crust are also characterized by protracted pre-breakup magmatism, which occurs over a substantially longer time span than at fast extension rates, despite the limiting effect of higher conductive cooling rate. For example, models with initially 45 km crust reach the point of crustal breakup within <25 Ma at 2 cm/a extension rate (except the case with no initial slab), and are magmatically active 10–20 Ma before breakup (Fig. 5). With 0.25 cm/a of extension, the time of breakup is increased by a factor of ~4, and 2–4 km magmatic crust is continuously produced from 50 Ma before breakup. Models with thicker crust and slow extension produce less localized thinning in both the crust and the mantle lithosphere, and even less magmatism. The effects observed in models with slow extension are essentially akin to the greater time available for ductile deformation to occur as well as the increased efficiency of

conductive cooling. Compared to the faster extension models, this means that less brittle deformation is required to accommodate lithosphere thinning, and both crustal and serpentinite flows become relatively more predominant, enhancing the abovementioned effects on strain distribution during rifting in the scenarios with different initial crustal thickness.

An additional difference from the models with faster extension is that small-scale convective erosion driven by horizontal thermal gradients due to lithosphere thinning (e.g. Buck, 1986) is more pronounced when thinning is slow (Fig. 7). The convective erosion is more efficient in this case, because there is more time for convective instabilities to grow. Besides thermal gradients, the convective erosion is also driven and enhanced by the presence of relatively dense eclogite from the margins where the eclogite was initially deepest. As the geotherm is vertically compressed during extension, the eclogite is heated by conduction, so effective viscosity is reduced, and eventually the eclogite is delaminated along with the surrounding mantle lithospheric mantle.
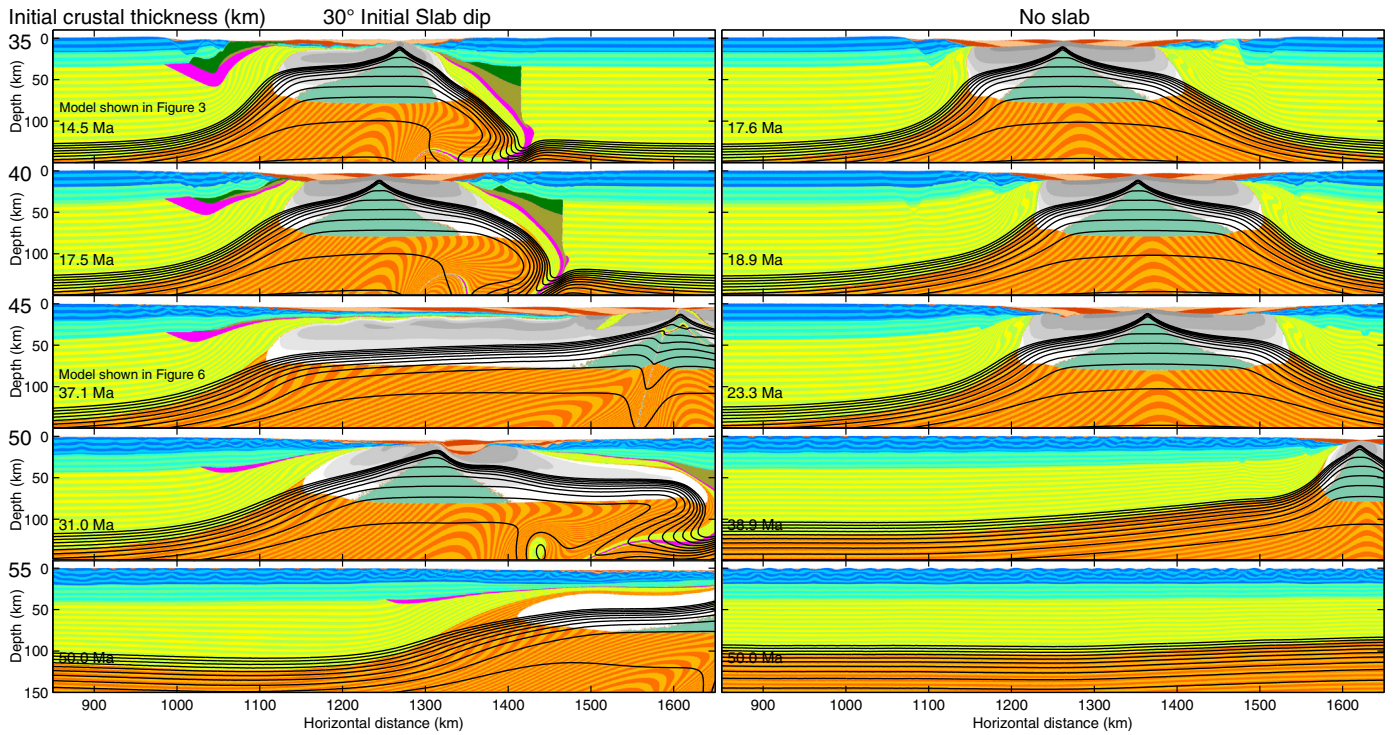
Fig. 4. Models with extension rate of 2 cm/a, different crustal thickness and either with or without a fossil slab and mantle wedge. The panels show stages corresponding to either 10 Ma after continental breakup (defined as the time where crustal thinning factor, β, somewhere exceeds 100) or at the 50 Ma maximum simulation time. Colors are as in Fig. 3. (For interpretation of the references to color in this figure legend, the reader is referred to the web version of this article.)
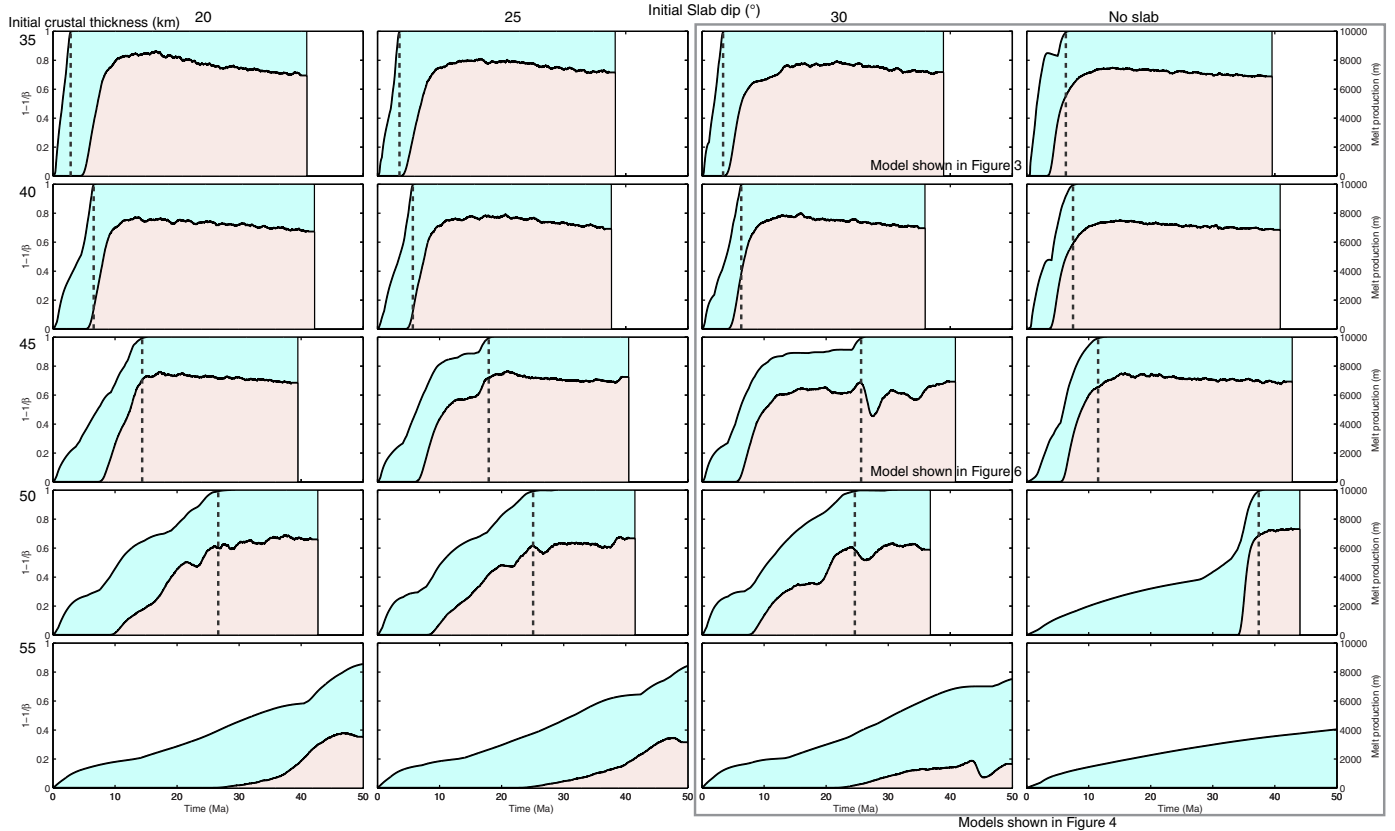

Fig. 5. Stretch factor, $1-1/\beta$ (blue) and integrated melt production thickness (grayish pink) as functions of model time for all models with extension rate of 2 cm/a. Vertical dashed line corresponds to the time of continental breakup. Lithological cross sections of some of the models can be found in Fig. 4. All cross sections are presented in Fig. S2. (For interpretation of the references to color in this figure legend, the reader is referred to the web version of this article.)
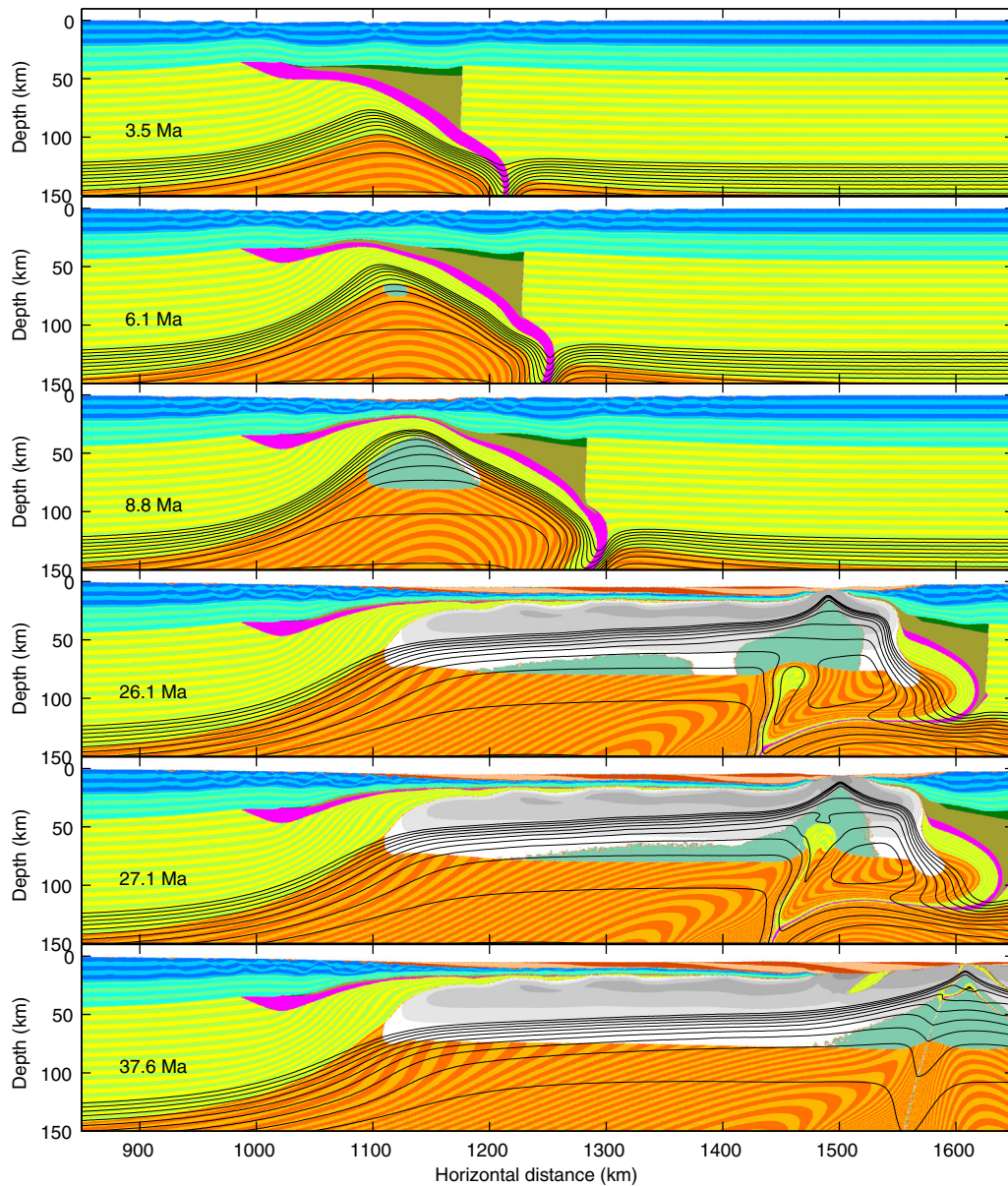
Fig. 6. Evolution of model with initially 45 km crust and fossil slab dip of 30°. Colors as in Fig. 3. (For interpretation of the references to color in this figure legend, the reader is referred to the web version of this article.)

Comparison of Figs. 4 and 7 for models with initially 35 km crust and 30° slab dip, for example, shows that for slow extension the eclogite on the right margin side has been almost completely eroded, whereas for the fast extension case most of the eclogite is preserved at the time of break-up. The convective erosion also manifests in enhanced melt production and 1–2 km transient variation of melt-production rates for the slowly extending models (Fig. 8). This is not present in the slowly extending models with no initial slab (Fig. 8; rightmost column), and only to a lesser extent in the models with faster extension and an initial slab (Fig. 5).

4.4. Effect of the dip angle

The effect of the dip angle (Fig. S3) is not as pronounced as the effect of crustal thickness or extension rate. Clearly, the dip angle determines the absolute amount of serpentinite given our assumed initial geometry and thereby the eclogite–serpentinite ratio (higher ratio at low angle and smaller ratio at steep angle). This has the effect that serpentinite bodies below the thinned crust are less voluminous at steeper angles. A second effect is that rifting localizes further away from the

impingement of the slab at Moho depth with flatter angles, so that the slab is preserved further inland compared to the case where the slab is steep and rifting localizes closer to the slab.

5. Discussion

It is likely a characteristic feature of rifted margins, which have undergone pre-extensional collisional events, that rifting initiated along such older collision-related structures (Williams, 1995; Buiter and Torsvik, 2014). Extension of orogenic lithosphere with our assumed initial configuration with a fossil eclogite slab, a fossil serpentinized mantle wedge and thickened crust indeed leads to localization of rifting in the former orogen. Other explanations include pervasive anisotropic crystalline fabric within the mantle lithosphere (Vauchez et al., 1997).

Furthermore, our models imply that pre-rift orogenic properties impose a strong control on the thermo-mechanical rift to drift evolution during extension. For example, a variable such as the crustal thickness at the onset of extension controls whether magmatism initiates before or after breakup of the continental crust. For a thin crust, extension
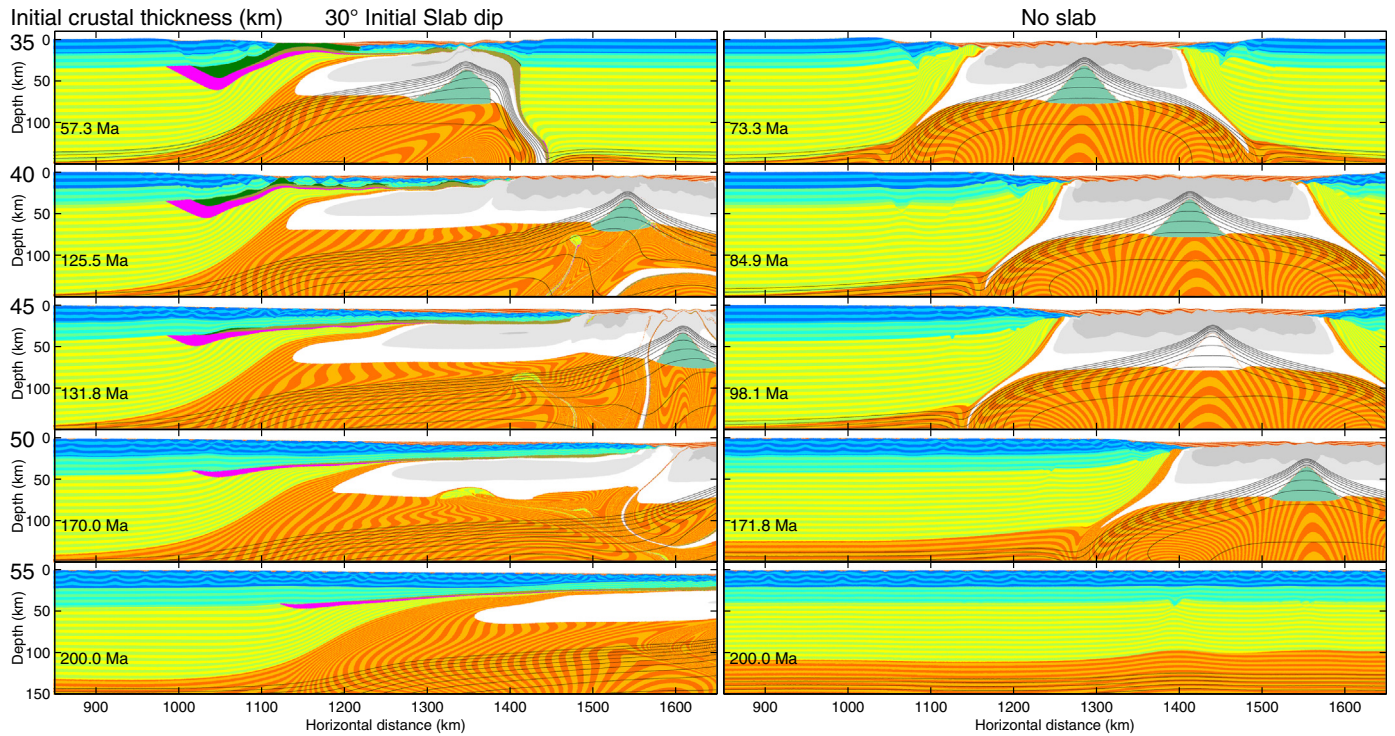
Fig. 7. Like Fig. 4, but for a slower extension rate of 0.5 cm/a. The plot times in this case correspond to either 40 Ma after continental breakup or a maximum simulation time of 200 Ma.

produces rapid crustal thinning and exhumation of serpentinite, before any melt is produced by decompression of the asthenosphere below (see Figs. 5 and 8 with initial crustal thickness of 35 km and Fig. 3).

The resulting conjugate margins are therefore essentially magma-poor. In contrast, for thicker crust, magmatism precedes break-up of the crust (see Figs. 5 and 8 with initial crustal thickness ≥35 km), and
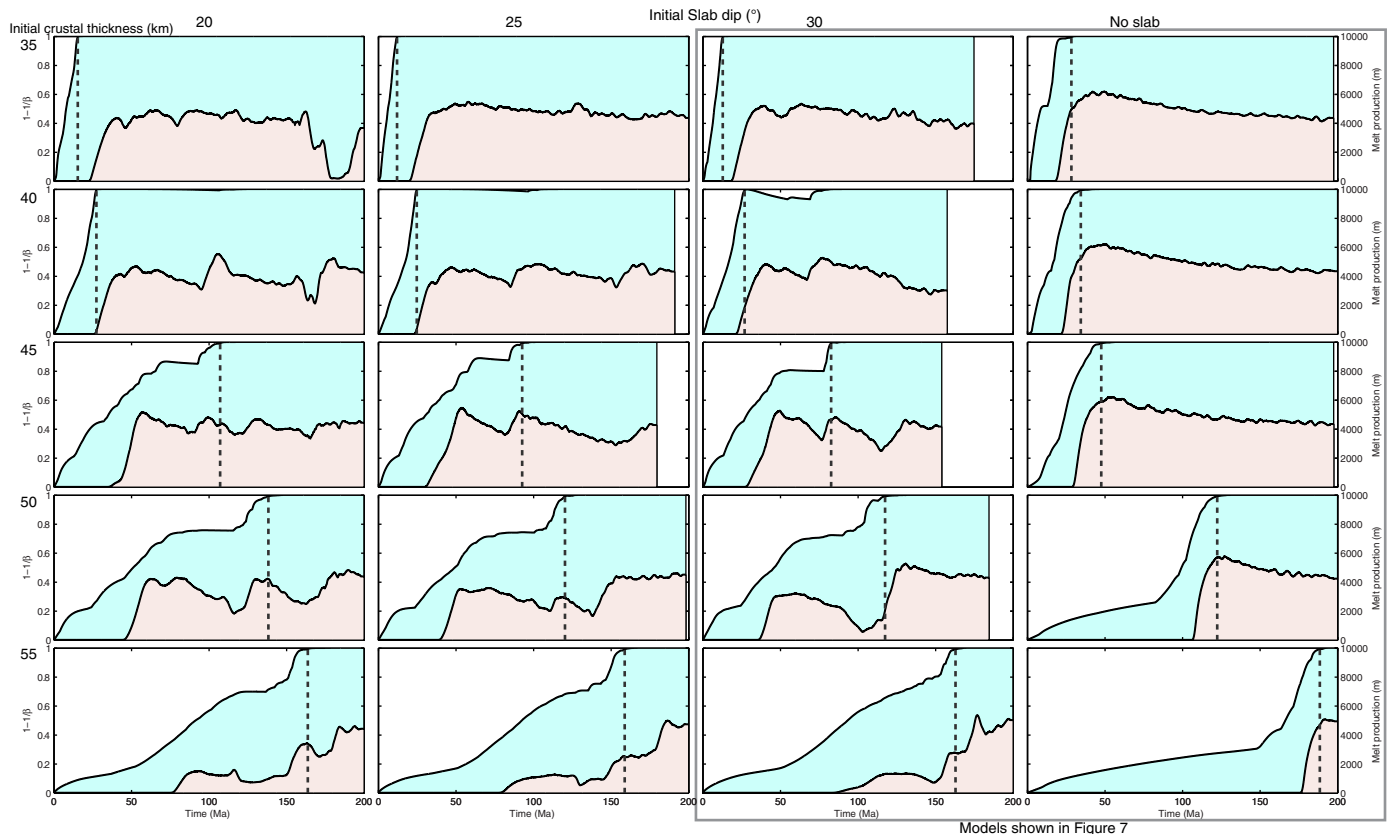

Fig. 8. Like Fig. 5, but for a slower extension rate of 0.5 cm/a. Lithological cross sections of some of the models can be found in Fig. 7. All cross sections are presented in Fig. S3.

several km of magmatic rocks with seaward-dipping isochrons are emplaced on top of the thinned continental crust (e.g. Fig. 6). This is a characteristic property of magma-rich margins (Menzies, 2002). We therefore propose that the thickness of the pre-rift crust controls whether passive margins become magma-rich or magma-poor. Inspection of regional crustal thickness along North Atlantic margins appears to support this hypothesis. The onshore crustal thickness of Iberia and Newfoundland is in the order of 35 km (Fig. 1), and the associated passive margins are magma-poor (Tucholke et al., 2007). Similarly, the Greenland–Norway continental margins are magma-rich (Mjelde et al., 2008), and onshore crustal thickness reaches 45–50 km.

Another important cause for the development of magma-poor margins, besides thinner crust, is the presence of orogenic serpentinite. Its buoyancy and low ductile strength facilitate rapid exhumation that enhances localized deformation of the crust. Initial crustal thickness is therefore also a primary control on the amount of preserved orogenic serpentinite, because 1) thin crust means more space for a hydrated mantle above the slab, and 2) crustal thickness affects sub-crustal thermal structure due to burial and radiogenic heat production and thereby the stability limit of serpentinite. Our models do demonstrate that a fossil orogenic serpentinized mantle wedge may be partially preserved beneath thinned continental crust, and become exhumed during subsequent continental breakup. This is driven by the buoyancy and the low viscosity of serpentinite. Existing models (e.g. Pérez-Gussinyé and Reston, 2001) attribute the presence of serpentinite to hydration facilitated by rift-related faulting. However, our modeling experiments imply the alternative explanation that the serpentinite (or some of it) is instead the exhumed remnant of an orogenic mantle wedge. In this context the lower limit of serpentinite could be explained as the stability limit of serpentinite-minerals rather than a hydration front (e.g. Pérez-Gussinyé and Reston, 2001). This explanation is consistent with oxygen isotope data from serpentinized mantle rocks off Iberia implying that serpentinization primarily occurred at relatively high temperatures, before exhumation and beneath continental crust (Skelton and Valley, 2000).

In models with little serpentinite present in the beginning, the orogenic serpentinite tends to stabilize at the base of thinned continental crust, instead of piercing the crust, causing break-up and mantle exhumation as seen in models with thinner initial crust and more initial serpentinite. However, in both models the resulting serpentinite bodies at the base of the continental crust could provide an additional explanation for the formation of some LCBs.

In the models presented, the amount of initial serpentinite is parameterized in terms of crustal thickness. In reality, the amount of the serpentinite would also depend on the thermal evolution from the end of subduction until extension and beyond as well as the degree of hydration and geometry of the mantle wedge during subduction. Also, complete breakdown of serpentine does not lead to complete dehydration, but may render the mantle with dissolved water that reduces viscosity (Mei and Kohlstedt, 2000). It has been proposed that such subduction-derived water causes weakening that allows for subduction initiation along passive margins, even 200–300 Ma after dehydration of the slab (van der Lee et al., 2008). These complexities are beyond the scope of this study, but will be accounted for in future work using models of margins that are involved in one or more full Wilson cycle. The model results presented in this paper imply that subduction-derived water may also play an important role during rift initiation.

An additional component of our models is the presence of a fossil subducted slab of eclogitized oceanic crust at the onset of rifting. Compared to crustal rocks and serpentinite, the ductile strength of eclogite differs much less from olivine-rich rocks present in the lithospheric mantle (Fig. 2), and the slab therefore has a lesser control on the large-scale evolution during extension. Therefore, generally the slab is passively advected along with the hosting mantle lithosphere during rifting and breakup. For models with relatively thin crust much of the original structure of the slab is preserved upon breakup, and either of the conjugated margins are rendered with an eclogite layer dipping in the opposite direction relative to the sea. This result demonstrates that such fossil slabs can retain some of their original structure upon extension. A possible example of this process is evident within the East Greenland continental margin (Fig. 1a; Schiffer et al., 2014; Schiffer et al., 2015b) where a seaward-dipping, possibly Caledonian mantle structure has been observed. Also the Flannan structure offshore Northern Scotland was interpreted to represent such a remnant slab, which survived rifting (e.g. Fig. 1c; Snyder and Flack, 1990; Warner et al., 1996; Schiffer et al., 2015b). Models with thicker crust tend to produce rifted margins where the shallow part of the slab is instead stretched along the base of the crust (Fig. 6). It has previously been suggested that North Atlantic LCBs with higher than normal upper mantle velocities (i.e. >8.2 km/s) may represent inherited collision-related metamorphics (Christiansson et al., 2000; Mjelde et al., 2013b). Our models confirm that such LCBs indeed may form during continental breakup, similar to the deformation and emplacement of orogenic serpentinite bodies, as described above. Such bodies are both possible candidates for the interpretation of high velocity bodies at Moho depth.

Recent studies have shown that hyperextension is an apparently common property of passive margins, i.e. the continental crust has been highly stretched to form a transition from continental to oceanic domains by up to several 100 km (Péron-Pinvidic and Manatschal, 2010; Lundin and Doré, 2011; Andersen et al., 2012). In the context of our modeling results, we note that post-orogenic extension of either endmember situations with thin or thick initial crust, respectively, produces hyperextension of different styles. However, the processes that lead to hyperextension differ. For thick initial crust, hyperextension is caused by flow in the crust that counteracts crustal thinning due to extension (e.g. Buck, 1991). This causes faster breakup (complete thinning) of the mantle lithosphere than the crust and wide and asymmetric margins with strongly stretched crust superimposed on asthenospheric mantle (Fig. 6). Similar crustal flow models have been invoked to explain hyperextension of magma-poor margins (Huismans and Beaumont, 2011; Brune et al., 2014), and whereas such models indeed predict realistic first-order crustal geometry, they are less consistent with observational constraints from hyperextended, magma-poor margins by two means: 1) They imply a pre-breakup onset of melt-generation, and 2) they do not produce exhumation of lithospheric mantle and/or thinned extensional allochthons of continental crust. The former is problematic, because the thickness of magmatic rocks in magma-poor margins, such as Iberia–Newfoundland, is much less than what can be explained by uniform lithospheric thinning (Minshull et al., 2001), a process that would produce even less pre-breakup melt than if the mantle lithosphere breaks up before the crust. The latter may even be more critical, because continental mantle exhumation, associated with extensional allochthons, appears to be a ubiquitous property of magma-poor margins (e.g. Péron-Pinvidic and Manatschal, 2010). However, the type of hyperextension associated with extension of lithosphere with thinner crust and pre-existing orogenic serpentinite as presented here (Fig. 3) is consistent with such observations from magma-poor margins, both in terms of 1) the lack of pre-breakup magmatism, 2) exhumation of (serpentinized) continental mantle and 3) the formation of extensional allochthons.

The models presented here indicate that rheological inhomogeneity due to certain orogenic structures can explain many aspects of the evolution of passive margins. It is however also likely that additional complexity involved in the state of the lithosphere at onset of extension should be accounted for. For example, Yamasaki and Gernigon (2009) attributed rift localization and evolution to rheological heterogeneity due to the presence of pre-rift mafic intrusions in the lower crust, and Huismans and Beaumont (2011) accounted for the presence of buoyant cratonic mantle lithosphere and showed that, under certain boundary and initial conditions, it would be exhumed during rifting.

This implies that, in order to explain particular passive margins in greater detail than in the present paper, additional local geological constraints should be employed in a corresponding numerical model. Also, there are exceptions to the general feature that margins tend to develop parallel to pre-existing structures. For example, the Caledonian margin in Greenland appears to cut across older Proterozoic and Archean trends (Williams, 1995), and the present-day Charlie Gibbs transform is aligned with the Iapetus suture (Williams, 2003; Buiter and Torsvik, 2014). Initial opening of the South Atlantic followed older Pan-African sutures, but eventually cutting through the Congo–São Francisco Craton, ignoring the sutures (Buiter and Torsvik, 2014). We speculate that although rifting generally occurs parallel to old sutures, other effects may sometimes modulate the process. These may include local variations in strength and both local and far-field stress variations.

Further modeling efforts, possibly accounting for 3D effects (e.g. strength variations between cratonic and weaker lithosphere and boundary conditions reflecting different stress states) may therefore be needed in order to understand such complexities, with emphasis on those conditions that lead to structural inheritance and parallelism and those that do not.

6. Conclusions

1. It is mechanically feasible that passive margin formation and evolution can be controlled by the presence of pre-existing orogenic structures.

2. Serpentinite, often forming the crystalline basement of distal zones of magma-poor margins, can be explained by exhumation of fossil mantle wedge material formed during pre-rift subduction of oceanic crust.

3. Similarly, fossil mantle wedge material can also become emplaced at the base of thinned continental crust and form LCBs with typically higher than crustal, but lower than mantle velocities.

4. Fossil slab material entrained in the lithospheric mantle at the onset of extension is rheologically similar to the hosting mantle lithosphere and does not cause intense strain localization upon extension. It may therefore 'survive' extension and either break passively apart to form two dipping structures in the mantle lithosphere of each conjugate margin, or it may become sheared along the Moho on the side of the rift where the slab was shallowest. In that case a dipping structure consisting of the initially deeper part of the slab is preserved on the conjugate side. In either case, the initially shallowest part of the slab deforms to form structures at the base of the crust with possibly higher than mantle velocities.

5. Crustal thickness imposes an important control on the relative timing of melting and crustal breakup, respectively. If initial crust is relatively thick (>45 km) at the onset of extension, thinning of the mantle lithosphere is more efficient than crustal thinning, and decompression melting may onset before crustal breakup, erupting km-thick flood basalts onto the thinned continental crust. On the other hand, if the crust is initially thin orogenic serpentinite may remain stable in the uppermost mantle which leads to rapid rift localization, during extension, and crustal breakup occurs before the onset decompression melting. These two different scenarios can occur above sub lithospheric mantle with the same potential temperature.

6. Hyperextension with crustal allochthons separated by exhumed mantle, often observed in magma-poor margins, can be explained by extension of continental crust with pre-rift serpentinite preserved below (e.g. a fossil mantle wedge). This is a novel result. On the other hand, hyperextension (by means of extremely thinned continental crust) can be explained by crustal flow and pronounced rift delocalization in thick continental crust. This is in accord with previous modeling studies. Both models produce asymmetry of the conjugate margin pairs.

Appendix A. Supplementary data

Supplementary data to this article can be found online at http://dx.doi.org/10.1016/j.gr.2016.06.012.

References

Andersen, T.B., Corfu, F., Labrousse, L., Osmundsen, P.-T., 2012. Evidence for hyperextension along the pre-Caledonian margin of Baltica. Journal of the Geological Society 169, 601–612.

Aoki, I., Takahashi, E., 2004. Density of MORB eclogite in the upper mantle. Physics of the Earth and Planetary Interiors 143–144, 129–143.

Balling, N., 2000. Deep seismic reflection evidence for ancient subduction and collision zones within the continental lithosphere of northwestern Europe. Tectonophysics 329, 269–300.

Berman, R.G., Brown, T.H., 1986. Heat capacity of minerals in the system Na₂O–K₂O–CaO–MgO–FeO–Fe₂O₃–Al₂O₃–Sio₂–TiO₂–H₂O–CO₂: representation, estimation, and high temperature extrapolation. Contributions to Mineralogy and Petrology 94, 262.

Boillot, G., Grimaud, S., Mauffret, A., Mougenot, D., Kornprobst, J., Mergoil-Daniel, J., Torrent, G., 1980. Ocean–continent boundary off the Iberian margin: a serpentinite diapir west of the Galicia Bank. Earth and Planetary Science Letters 48, 23–34.

Bostock, M., Hyndman, R., Rondenay, S., Peacock, S., 2002. An inverted continental Moho and serpentinization of the forearc mantle. Nature 417, 536–538.

Boutilier, R., Keen, C., 1999. Small-scale convection and divergent plate boundaries. Journal of Geophysical Research: Solid Earth (1978–2012) 104, 7389–7403.

Bown, J.W., White, R.S., 1994. Variation with spreading rate of oceanic crustal thickness and geochemistry. Earth and Planetary Science Letters 121, 435–449.

Brun, J., Beslier, M., 1996. Mantle exhumation at passive margins. Earth and Planetary Science Letters 142, 161–173.

Brune, S., Heine, C., Pérez-Gussinyé, M., Sobolev, S.V., 2014. Rift migration explains continental margin asymmetry and crustal hyper-extension. Nature Communications 5.

Buck, R.W., 1986. Small-scale convection induced by passive rifting: the cause for uplift of rift shoulders. Earth and Planetary Science Letters 77, 362–372.

Buck, W.R., 1991. Modes of continental lithospheric extension. Journal of Geophysical Research 96, 20161–20178.

Buiter, S.J.H., Torsvik, T.H., 2014. A review of Wilson Cycle plate margins: a role for mantle plumes in continental break-up along sutures? Gondwana Research 26, 627–653.

Buiter, S.J.H., Babeyko, A.Y., Ellis, S., Gerya, T.V., Kaus, B.J.P., Kellner, A., Schreurs, G., Yamada, Y., 2006. Comparison of model results for a shortening and an extension experiment. Geological Society Special Publication 29–64.

Cawood, P.A., 2006. Precambrian plate tectonics: criteria and evidence. GSA Today 16, 4.

Christensen, N.I., Mooney, W.D., 1995. Seismic velocity structure and composition of the continental crust: a global view. Journal of Geophysical Research 100, 9761–9788.

Christiansson, P., Faleide, J., Berge, A., 2000. Crustal structure in the northern North Sea: an integrated geophysical study. Geological Society, London, Special Publications 167, 15–40.

Coffin, M.F., Eldholm, O., 1994. Large igneous provinces: crustal structure, dimensions, and external consequences. Reviews of Geophysics 32, 1–36.

Crameri, F., Schmeling, H., Golabek, G., Duretz, T., Orendt, R., Buiter, S., May, D., Kaus, B., Gerya, T., Tackley, P., 2012. A comparison of numerical surface topography calculations in geodynamic modelling: an evaluation of the 'sticky air' method. Geophysical Journal International 189, 38–54.

Cruciani, C., Carminati, E., Doglioni, C., 2005. Slab dip vs. lithosphere age: no direct function. Earth and Planetary Science Letters 238, 298–310.

Dewey, J., Spall, H., 1975. Pre-Mesozoic plate tectonics: how far back in Earth history can the Wilson Cycle be extended? Geology 3, 422–424.

Duesterhoeft, E., Quinteros, J., Oberhänsli, R., Bousquet, R., de Capitani, C., 2014. Relative impact of mantle densification and eclogitization of slabs on subduction dynamics: a numerical thermodynamic/thermokinematic investigation of metamorphic density evolution. Tectonophysics 637, 20–29.

Dunbar, J.A., Sawyer, D.S., 1989. How preexisting weaknesses control the style of continental breakup. Journal of Geophysical Research: Solid Earth 94, 7278–7292.

Duretz, T., Gerya, T.V., May, D.A., 2011. Numerical modelling of spontaneous slab breakoff and subsequent topographic response. Tectonophysics 502, 244–256.

Eddy, D.R., Van Avendonk, H.J.A., Shillington, D.J., 2013. Compressional and shear-wave velocity structure of the continent–ocean transition zone at the eastern Grand Banks, Newfoundland. Geophysical Research Letters 40, 3014–3020.

England, P., 1983. Constraints on extension of continental lithosphere. Journal of Geophysical Research 88, 1145–1152.

Fichler, C., Odinsen, T., Rueslätten, H., Olesen, O., Vindstad, J.E., Wienecke, S., 2011. Crustal inhomogeneities in the Northern North Sea from potential field modeling: inherited structure and serpentinites? Tectonophysics 510, 172–185.

143

Foulger, G.R., Jurdy, D.M., 2007. Plates, Plumes, and Planetary Processes. Geological
Society of America.
Foulger, G., Natland, J., Anderson, D., 2005. A source for Icelandic magmas in remelted
Iapetus crust. Journal of Volcanology and Geothermal Research 141, 23–44.
Froitzheim, N., Manatschal, G., 1996. Kinematics of Jurassic rifting, mantle exhumation,
and passive-margin formation in the Austroalpine and Penninic nappes (eastern
Switzerland). Geological Society of America Bulletin 108, 1120–1133.
Gee, D.G., Fossen, H., Henriksen, N., Higgins, A.K., 2008. From the early Paleozoic platforms
of Baltica and Laurentia to the Caledonide Orogen of Scandinavia and Greenland.
Episodes 31, 44.
Gernigon, L., Lucazeau, F., Brigaud, F., Ringenbach, J.-C., Planke, S., Le Gall, B., 2006. A
moderate melting model for the Vøring margin (Norway) based on structural obser-
vations and a thermo-kinematical modelling: implication for the meaning of the
lower crustal bodies. Tectonophysics 412, 255–278.
Gerya, T.V., Yuen, D.A., 2007. Robust characteristics method for modelling multiphase
visco-elasto-plastic thermo-mechanical problems. Physics of the Earth and Planetary
Interiors 163, 83–105.
Gillet, P., Richet, P., Guyot, F., Fiquet, G., 1991. High-temperature thermodynamic proper-
ties of forsterite. Journal of Geophysical Research 96.
Hall, J., Quinlan, G., Marillier, F., Keen, C., 1990. Dipping shear zones and the base of the
crust in the Appalachians, offshore Canada. Tectonophysics 173, 581–593.
Hilairet, N., Reynard, B., Wang, Y., Daniel, I., Merkel, S., Nishiyama, N., Petitgirard, S., 2007.
High-pressure creep of serpentine, interseismic deformation, and initiation of
subduction. Science 318, 1910–1913.
Holbrook, W.S., Larsen, H., Korenaga, J., Dahl-Jensen, T., Reid, I.D., Kelemen, P., Hopper, J.,
Kent, G., Lizarralde, D., Bernstein, S., 2001. Mantle thermal structure and active up-
welling during continental breakup in the North Atlantic. Earth and Planetary Science
Letters 190, 251–266.
Huismans, R., Beaumont, C., 2011. Depth-dependent extension, two-stage breakup and
cratonic underplating at rifted margins. Nature 473, 74–78.
Ito, G., Lin, J., Gable, C.W., 1996. Dynamics of mantle flow and melting at a ridge-centered
hotspot: Iceland and the Mid-Atlantic Ridge. Earth and Planetary Science Letters 144,
53–74.
Iwamori, H., 1998. Transportation of H$_2$O and melting in subduction zones. Earth and
Planetary Science Letters 160, 65–80.
Jamtveit, B., Brooker, R., Brooks, K., Larsen, L.M., Pedersen, T., 2001. The water content of
olivines from the North Atlantic Volcanic Province. Earth and Planetary Science
Letters 186, 401–415.
Karato, S.I., Wu, P., 1993. Rheology of the upper mantle: a synthesis. Science 260,
771–778.
Katz, R.F., Spiegelman, M., Langmuir, C.H., 2003. A new parameterization of hydrous
mantle melting. Geochemistry, Geophysics, Geosystems 4, 1073.
Kawakatsu, H., Watada, S., 2007. Seismic evidence for deep-water transportation in the
mantle. Science 316, 1468–1471.
Kelemen, P.B., Holbrook, W.S., 1995. Origin of thick, high-velocity igneous crust along the
U.S. East Coast Margin. Journal of Geophysical Research: Solid Earth 100,
10077–10094.
King, S.D., Anderson, D.L., 1998. Edge-driven convection. Earth and Planetary Science Let-
ters 160, 289–296.
Korenaga, J., 2004. Mantle mixing and continental breakup magmatism. Earth and Plane-
tary Science Letters 218, 463–473.
Korenaga, J., Kelemen, P.B., 2000. Major element heterogeneity in the mantle source of the
North Atlantic igneous province. Earth and Planetary Science Letters 184, 251–268.
Korenaga, J., Holbrook, W., Kent, G., Kelemen, P., Detrick, R., Larsen, H.C., Hopper, J., Dahl-
Jensen, T., 2000. Crustal structure of the southeast Greenland margin from joint
refraction and reflection seismic tomography. Journal of Geophysical Research:
Solid Earth (1978–2012) 105, 21591–21614.
Leslie, A.G., Smith, M., Soper, N., 2008. Laurentian margin evolution and the Caledonian
orogeny—a template for Scotland and East Greenland. Geological Society of
America Memoirs 202, 307–343.
Lister, G., Etheridge, M., Symonds, P., 1986. Detachment faulting and the evolution of pas-
sive continental margins. Geology 14, 246–250.
Lundin, E.R., Doré, A.G., 2011. Hyperextension, serpentinization, and weakening: a new
paradigm for rifted margin compressional deformation. Geology 39, 347–350.
Manatschal, G., 2004. New models for evolution of magma-poor rifted margins based on a
review of data and concepts from West Iberia and the Alps. International Journal of
Earth Sciences 93, 432–466.
Manatschal, G., Lavier, L., Chenin, P., 2015. The role of inheritance in structuring
hyperextended rift systems: some considerations based on observations and numer-
ical modeling. Gondwana Research 27, 140–164.
McKenzie, D., Jackson, J., Priestley, K., 2005. Thermal structure of oceanic and continental
lithosphere. Earth and Planetary Science Letters 233, 337–349.
Mei, S., Kohlstedt, D.L., 2000. Influence of water on plastic deformation of olivine aggre-
gates: 2. Dislocation creep regime. Journal of Geophysical Research: Solid Earth 105,
21471–21481.
Menzies, M.A., 2002. Volcanic Rifted Margins. Geological Society of America.
Minshull, T.A., Muller, M.R., Robinson, C.J., White, R.S., Bickle, M.J., 1998. Is the oceanic
Moho a serpentinization front? Geological Society, London, Special Publications
148, 71–80.
Minshull, T.A., Dean, S.M., White, R.S., Whitmarsh, R.B., 2001. Anomalous melt production
after continental break-up in the southern Iberia Abyssal Plain. Geological Society,
London, Special Publications 187, 537–550.
Mjelde, R., Kasahara, J., Shimamura, H., Kamimura, A., Kanazawa, T., Kodaira, S., Raum, T.,
Shiobara, H., 2002. Lower crustal seismic velocity-anomalies; magmatic underplating
or serpentinized peridotite? Evidence from the Vøring Margin, NE Atlantic. Marine
Geophysical Researches 23, 169–183.

Mjelde, R., Raum, T., Breivik, A., Faleide, J., 2008. Crustal transect across the North Atlantic.
Marine Geophysical Researches 29, 73–87.
Mjelde, R., Goncharov, A., Müller, R.D., 2013b. The Moho: boundary above upper mantle
peridotites or lower crustal eclogites? A global review and new interpretations for
passive margins. Tectonophysics 609, 636–650.
Mutter, J.C., Talwani, M., Stoffa, P.L., 1982. Origin of seaward-dipping reflectors in oceanic
crust off the Norwegian margin by "subaerial sea-floor spreading". Geology 10, 353–357.
Mutter, J.C., Buck, W.R., Zehnder, C.M., 1988. Convective partial melting: 1. A model for
the formation of thick basaltic sequences during the initiation of spreading. Journal
of Geophysical Research: Solid Earth 93, 1031–1048.
Nielsen, T.K., Hopper, J.R., 2004. From rift to drift: mantle melting during continental
breakup. Geochemistry, Geophysics, Geosystems 5, Q07003.
Olafsson, I., Sundvor, E., Eldholm, O., Grue, K., 1992. Møre margin: crustal structure from
analysis of expanded spread profiles. Marine Geophysical Researches 14, 137–162.
Parsons, B., Sclater, J.G., 1977. An analysis of the variation of ocean floor bathymetry and
heat flow with age. Journal of Geophysical Research 82, 803–827.
Pérez-Gussinyé, M., Reston, T.J., 2001. Rheological evolution during extension at nonvol-
canic rifted margins: onset of serpentinization and development of detachments
leading to continental breakup. Journal of Geophysical Research: Solid Earth
(1978–2012) 106, 3961–3975.
Péron-Pinvidic, G., Manatschal, G., 2009. The final rifting evolution at deep magma-poor
passive margins from Iberia–Newfoundland: a new point of view. International
Journal of Earth Sciences 98, 1581–1597.
Péron-Pinvidic, G., Manatschal, G., 2010. From microcontinents to extensional
allochthons: witnesses of how continents rift and break apart? Petroleum Geoscience
16, 189–197.
Petersen, K.D., Nielsen, S.B., Clausen, O.R., Stephenson, R., Gerya, T., 2010. Small-scale
mantle convection produces stratigraphic sequences in sedimentary basins. Science
329, 827–830.
Petersen, K., Armitage, J., Nielsen, S., Thybo, H., 2015. Mantle temperature as a control on
the time scale of thermal evolution of extensional basins. Earth and Planetary Science
Letters 409, 61–70.
Phipps Morgan, J., 1997. The generation of a compositional lithosphere by mid-ocean
ridge melting and its effect on subsequent off-axis hotspot upwelling and melting.
Earth and Planetary Science Letters 146, 213–232.
Phipps Morgan, J., Morgan, W.J., 1999. Two-stage melting and the geochemical evolution
of the mantle: a recipe for mantle plum-pudding. Earth and Planetary Science Letters
170, 215–239.
Piper, J.D.A., 2000. The Neoproterozoic supercontinent: Rodinia or Palaeopangaea? Earth
and Planetary Science Letters 176, 131–146.
Ranalli, G., 1995. Rheology of the Earth. second ed Chapman & Hall, London.
Ren, S., Skogseid, J., Eldholm, O., 1998. Late Cretaceous–Paleocene extension on the Vøring
volcanic margin. Marine Geophysical Researches 20, 343–369.
Reston, T.J., Morgan, J.P., 2004. Continental geotherm and the evolution of rifted margins.
Geology 32, 133–136.
Roberts, D., 2003. The Scandinavian Caledonides: event chronology, palaeogeographic
settings and likely modern analogues. Tectonophysics 365, 283–299.
Schiffer, C., Balling, N., Jacobsen, B.H., Stephenson, R.A., Nielsen, S.B., 2014. Seismological
evidence for a fossil subduction zone in the East Greenland Caledonides. Geology.
Schiffer, C., Jacobsen, B.H., Balling, N., Nielsen, S.B., 2015a. The East Greenland Caledonides —
teleseismic signature, gravity and isostasy. Geophysical Journal International.
Schiffer, C., Stephenson, R.A., Petersen, K.D., Nielsen, S.B., Jacobsen, B.H., Balling, N.,
Macdonald, D.I.M., 2015b. A sub-crustal piercing point for North Atlantic reconstruc-
tions and tectonic implications. Geology.
Scott, D.R., 1992. Small-scale convection and mantle melting beneath mid-ocean ridges.
Geophysical Monograph Series 71, 327–352.
Shirey, S.B., Richardson, S.H., 2011. Start of the Wilson cycle at 3 Ga shown by diamonds
from subcontinental mantle. Science 333, 434–436.
Skelton, A.D., Valley, J.W., 2000. The relative timing of serpentinisation and mantle exhu-
mation at the ocean–continent transition, Iberia: constraints from oxygen isotopes.
Earth and Planetary Science Letters 178, 327–338.
Skogseid, J., Planke, S., Faleide, J.I., Pedersen, T., Eldholm, O., Neverdal, F., 2000. NE Atlantic
continental rifting and volcanic margin formation. Geological Society, London, Special
Publications 167, 295–326.
Snyder, D.B., Flack, C.A., 1990. A Caledonian age for reflectors within the mantle litho-
sphere north and west of Scotland. Tectonics 9, 903–922.
Stamfli, G.M., Kozur, H.W., 2006. Europe from the Variscan to the Alpine cycles. Geological
Society of London's Memoirs 32, 57–82.
Tegner, C., Duncan, R.A., Brooks, C.K., Bird, D.K., Storey, M., 1998. $^{40}Ar^{39}Ar$
geochronology of Tertiary mafic intrusions along the East Greenland rifted margin:
relation to flood basalts and the Iceland hotspot track. Earth and Planetary Science
Letters 156, 75–88.
Thomas, W.A., 2006. Tectonic inheritance at a continental margin. GSA Today 16, 4–11.
Thybo, H., Artemieva, I.M., 2013. Moho and magmatic underplating in continental
lithosphere. Tectonophysics 609, 605–619.
Tucholke, B., Sawyer, D., Sibuet, J.-C., 2007. Breakup of the Newfoundland–Iberia rift.
Geological Society, London, Special Publications 282, 9–46.
Ulmer, P., Trommsdorff, V., 1995. Serpentine stability to mantle depths and subduction-
related magmatism. Science 268, 858–861.
van der Lee, S., Regenauer-Lieb, K., Yuen, D.A., 2008. The role of water in connecting past
and future episodes of subduction. Earth and Planetary Science Letters 273, 15–27.
van der Velden, A.J., Cook, F.A., 2005. Relict subduction zones in Canada. Journal of
Geophysical Research: Solid Earth 110, B08403.
van der Velden, A.J., Van Staal, C.R., Cook, F.A., 2004. Crustal structure, fossil subduction, and
the tectonic evolution of the Newfoundland Appalachians: evidence from a reprocessed
seismic reflection survey. Geological Society of America Bulletin 116, 1485–1498.

Van Staal, C., Dewey, J., Mac Niocaill, C., McKerrow, W., 1998. The Cambrian–Silurian tectonic evolution of the northern Appalachians and British Caledonides: history of a complex, west and southwest Pacific-type segment of Iapetus. Geological Society, London, Special Publications 143, 197–242.

van Wijk, J.W., Huismans, R.S., ter Voorde, M., Cloetingh, S.A.P.L., 2001. Melt generation at volcanic continental margins: no need for a mantle plume? Geophysical Research Letters 28, 3995–3998.

Vauchez, A., Barruol, G., Tommasi, A., 1997. Why do continents break-up parallel to ancient orogenic belts? Terra Nova 9, 62–66.

Warner, M., Morgan, J., Barton, P., Morgan, P., Price, C., Jones, K., 1996. Seismic reflections from the mantle represent relict subduction zones within the continental lithosphere. Geology 24, 39–42.

Wernicke, B., 1981. Low-angle normal faults in the Basin and Range Province: nappe tectonics in an extending orogen. Nature 291, 645–648.

White, R., 1992. Crustal structure and magmatism of North Atlantic continental margins. Journal of the Geological Society 149, 841–854.

White, R., McKenzie, D., 1989. Magmatism at rift zones: the generation of volcanic continental margins and flood basalts. Journal of Geophysical Research: Solid Earth (1978–2012) 94, 7685–7729.

White, R.S., Smith, L.K., Roberts, A.W., Christie, P.A.F., Kusznir, N.J., 2008. Lower-crustal intrusion on the North Atlantic continental margin. Nature 452, 460–464.

Williams, H., 1995. Geology of the Appalachian—Caledonian Orogen in Canada and Greenland. Geological Society of America.

Williams, H., 2003. Geologic ancestors to the Atlantic: the geology of Newfoundland. Newfoundland Quaterly 96.

Wilson, J.T., 1966. Did the Atlantic close and then re-open? Nature 211, 676–681.

Yamasaki, T., Gernigon, L., 2009. Styles of lithospheric extension controlled by underplated mafic bodies. Tectonophysics 468, 169–184.

Zhang, J., Green, H.W., 2007. Experimental investigation of eclogite rheology and its fabrics at high temperature and pressure. Journal of Metamorphic Geology 25, 97–115.